Construction and Building Materials 48 (2013) 1240–1247

Contents lists available at SciVerse ScienceDirect

Construction and Building Materials

journal homepage: www.elsevier.com/locate/conbuildmat

Corrosion mechanisms in reinforced concrete by acoustic emission

Yuma Kawasaki [a,*], Tomoyo Wakuda [b], Tomoe Kobarai [b], Masayasu Ohtsu [b]

[a] Department of Civil and Environmental Engineering, Ritsumeikan University, Japan
[b] Graduate School of Science and Technology, Kumamoto University, Japan

HIGHLIGHTS

- We have identified two periods at the onset of corrosion in rebar and the nucleation of corrosion-induced cracks in concrete.
- Quantitative information on locations and kinematics of cracks is inherently necessary for diagnosis of concrete structures.
- This research aims at a hybrid NDE of AE and electrochemical methods for on-site monitoring of corrosion damages in concrete.

ARTICLE INFO

Article history:
Available online 29 March 2013

Keywords:
Acoustic emission
Corrosion-induced cracks
EPMA
Ib-value
SiGMA

ABSTRACT

Continuous acoustic emission (AE) monitoring is applied to a cyclic wet and dry test of reinforced concrete beams. The onset of corrosion and the nucleation of corrosion-induced cracks in concrete are successfully identified, and then, cross-sections inside the concrete specimen are observed by an electron probe micro analyzer (EPMA). Results of AE parameter analysis are compared with the corrosion mechanisms observed by EPMA. Further, a relation between kinematical information of AE sources and nucleation of micro-cracks inside is identified by the SiGMA analysis and observed by the stereo-microscope. From these results, AE is a promising technique to quantitatively evaluate the corrosion process in concrete due to expansion of corrosion products at an early stage is demonstrated.

Published by Elsevier Ltd.

1. Introduction

Corrosion problems of reinforcing steel bar (rebar) in reinforced concrete (RC) by salt attack have been widely reported through-out the world. Basically, concrete provides a good durable condition for embedded rebar with high alkaline environment by forming a passive film on the surface of rebar. Due to ingress of chloride ions through concrete, the pas-sive film is destroyed and corrosion is initiated.

In order to avoid harmful damages, many monitoring methods have been developed to evaluate the corrosion before reaching the critical level [1]. One effective method could be nondestructive testing (NDT). NDT techniques are practical and useful in both a laboratory test and on-site measurement. So far, such electrochemical techniques as half-cell potential, polarization resistance and so forth are widely employed. Recently, acoustic emission (AE) is introduced for detecting both the onset of corrosion and the corrosion-induced cracks in concrete [2].

According to the phenomenological model of steel corrosion in seawater environments, it is reported [3] that a typical corrosion loss (loss of mass) during the corrosion process can be divided into four phases shown in Fig. 1. At Phase 1, the onset of corrosion is initiated. Activity of the corrosion process is dominated by the rate of penetration of oxygen and water. Then a corrosion loss decreases at Phase 2, because the flow of oxygen is eventually inhibited by rust on the surface of rebar. The mass loss due to corrosion increases again at Phase 3, because the corrosion penetrates inside and the expansion of corrosion products occurs. Eventually, the corrosion progresses at an almost constant speed at Phase 4. Thus, the phenomenological model is characterized by two transition phases of the onset of corrosion and the growth of corrosion products. Since the latter could generate the corrosion-induced cracks in concrete, acoustic emission (AE) was introduced. It has been demonstrated that both the onset of corrosion in rebar and the nucleation of cracks in concrete due to expansion of corrosion products are successfully detected by AE [2].

In the present paper, AE activities under a cyclic wet and dry test are investigated and these results are confirmed by an electron probe micro analyzer (EPMA). In order to investigate kinematical information of AE sources and nucleation of micro-cracks inside concrete, AE sources due to rebar corrosion in reinforced concrete are identified by the SiGMA (Simplified Green's functions for Moment tensor Analysis) analysis and cracks are observed by the stereo-microscope. In addition, characteristics of AE signals are investigated by using AE parameter analysis [4] including

* Corresponding author. Address: Department of Civil and Environmental Engineering, Ritsumeikan University, Noji-Higashi 1-1-1, Kusatsu, Shiga 525-8577, Japan. Tel.: +81 77 561 3368.
E-mail address: yuma-k@fc.ritsumei.ac.jp (Y. Kawasaki).

0950-0618/$ - see front matter Published by Elsevier Ltd.
http://dx.doi.org/10.1016/j.conbuildmat.2013.02.020

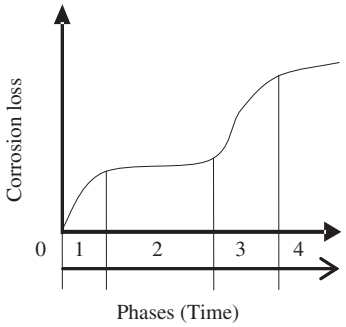

Fig. 1. Evaluation of corrosion loss in steel under seawater immersion.

Ib-value analysis [5]. Thus, quantitative comparison is performed. From these results, a promise for AE techniques to detect corrosion-induced cracks in concrete is demonstrated.

2. Experimental procedure

2.1. Specimens

Configuration of a specimen is illustrated in Fig. 2. Three beams of dimensions 100 mm × 75 mm × 400 mm were made. A deformed rebar of 13 mm nominal diameter is embedded with 20 mm cover-thickness. Ordinary Portland cement (OPC) was used. Coarse aggregate (gravel) was granite, of which the maximum gravel size is 10 mm. Concerning mixture proportion, the ratios of water, cement, sand, and gravel were 0.55, 1.0, 2.57, and 3.01 by weight. The slump value and air content of fresh concrete were controlled by admixture as 80 mm and 5.0%, respectively. To accelerate corrosion of rebar, 0.21 kg NaCl was mixed in water.

After water curing for 28 days in 20 °C water, chloride content was measured in one cylindrical sample of 100 mm diameter and 200 mm height. It was found that chloride content was 0.325 kg per 1 m^3 concrete as 0.052% mass of cement. A compressive strength of concrete at 28 days was 43.9 MPa, which was obtained as an averaged value from three cylindrical samples of 100 mm diameter and 200 mm height.

2.2. Cyclic wet and dry test

Following water curing for 28 days, a corrosion process due to salt attack was simulated by a cyclic wet and dry test. All these beams were cyclically placed into a container filled with 3% NaCl solution for a week and subsequently taken out of the container to dry under ambient temperature for another week, as shown in Fig. 3.

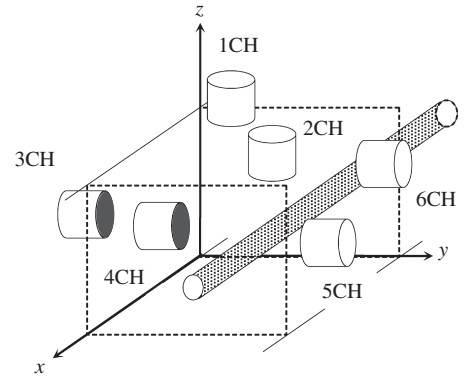

Fig. 4. Set of AE sensors.

Table 1
Coordinates of AE sensors.

	x (m)	*y* (m)	*z* (m)
1CH	0.010	0.030	0.075
2CH	0.100	0.070	0.075
3CH	0.090	0.000	0.045
4CH	0.020	0.000	0.030
5CH	0.095	0.100	0.033
6CH	0.010	0.100	0.055

In one beam, AE measurement was continuously conducted using an AE measuring system (DiSP, PAC). Six AE sensors (R15, PAC) of 150 kHz resonance are attached to the surface of the beam as shown in Fig. 4. The coordinates of all AE sensors are given in Table 1. The frequency range of the measurement was 10 kHz to 2 MHz. AE signals were amplified with 40 dB gain in a pre-amplifier and 20 dB gain in a main amplifier. For ringdown-counting, the dead-time was set to 2 ms and the threshold level to 40 dB gain.

Every week, AE measurement was temporarily stopped to conduct a half-cell potential measurement. At the center of the bottom surface in the beam the potential was measured by using a portable corrosion meter, (SRI-CM-II) [6] once, and C. S. E. values were estimated on the basis of ASTM C876 standard [7].

After AE measurement, the other two beams were cut and SEM (Scanning Electron Micrograph) observation was conducted to investigate microstructures around the rebar.

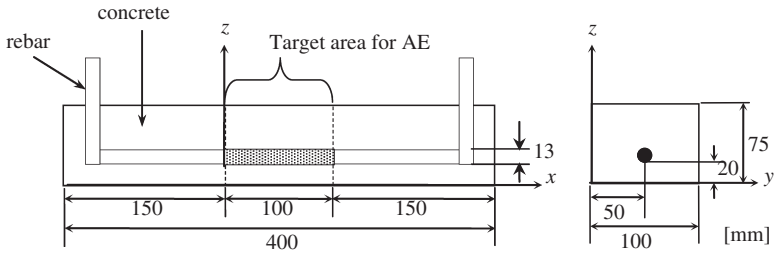

Fig. 2. Sketch of reinforced concrete beam tested.

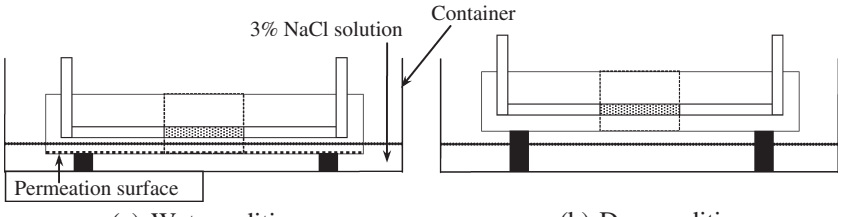

Fig. 3. Sketch of cyclic wet and dry test.

3. Analytical procedure

3.1. AE parameter

AE signals detected are analyzed by employing AE parameters of count, event, maximum amplitude, rise-time and duration as illustrated in Fig. 5. Characteristics of AE signals are particularly estimated by using two indices of RA value and average frequency, which are defined as [8],

$$\text{RA value} = \text{Rise time}/\text{Maximum Amplitude} \quad (1)$$

$$\text{Average frequency} = \text{AE Counts}/\text{Duration time} \quad (2)$$

3.2. Ib-value analysis

In order to evaluate the size distribution of AE sources, an amplitude distribution of AE hits is analyzed. A relationship between the number of AE hits, N, and the maximum amplitudes, A, is statistically represented as,

$$\text{Log}_{10}N = \alpha - b\,\text{Log}_{10}N \quad (3)$$

where α and b are empirical constants. For the latter, so-called improved b value (Ib-value) is adopted for calculation, based on cumulative distribution [5]. For 100 AE hits, the Ib-value is defined, assuming averaged amplitude μ and standard deviation σ,

$$Ib = \frac{[\log_{10}N(\mu - \alpha_2\sigma) - \log_{10}N(\mu + \alpha_1\sigma)]}{(\alpha_1 + \alpha_2)\sigma} \quad (4)$$

where $N(\mu - \alpha_2\sigma)$ and $N(\mu + \alpha_1\sigma)$ represent the number of hits with the amplitudes higher than $\mu - \alpha_2\sigma$ and $\mu + \alpha_1\sigma$, respectively. In the case that the Ib-values are large, small AE hits are mostly generated.

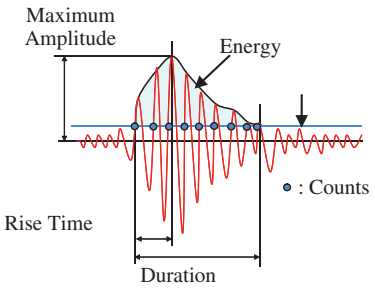

Fig. 5. AE waveform parameters.

In contrast, the case where the Ib-values become small implies nucleation of large AE hits.

3.3. SiGMA analysis

To study mechanisms of corrosion-induced cracks, SiGMA procedure for AE waveform analysis is applied [9]. SiGMA analysis consists of three-dimensional AE source location procedure and moment tensor analysis for AE sources. The location of the AE source is determined from the arrival time differences. Then, the components of the moment tensor are determined from the amplitudes of first motions at 6 channels. The classification of a crack is performed by the eigenvalue analysis of the moment tensor. Crack motions on the crack surface are assumed to be composed of slip motions (shear components) and crack-opening motions (tensile components), as illustrated in Fig. 6. Setting the maximum shear contribution of the moment tensor as X, three eigenvalues for a pure shear crack, e_1, e_2, and e_3, become X, 0, $-X$. Likewise in the case of a pure tensile crack, three eigenvalues are decomposed into deviatoric components Y, $-Y/2$, $-Y/2$ and isotropic (hydrostatic mean) components Z, Z, Z, when the ratio of the maximum deviatoric tensile component is set as Y and the isotropic tensile as Z. For a general crack, it is assumed that the eigenvalues of the moment tensor consist of both shear and tensile cracks. Thus, for classification of a general crack, Eq. (5) is derived [10,11]:

$$\begin{aligned} 1.0 &= X + Y + Z \\ e_{12} &= 0 - 0.5Y + Z \\ e_{13} &= -X - 0.5Y + Z \end{aligned} \quad (5)$$

where e_{12} is the ratio of the intermediate eigenvalue to the maximum eigenvalue, and e_{13} is the ratio of the minimum eigenvalue to the maximum.

In the SiGMA code, AE sources for which the shear ratios X are smaller than 40% are classified as tensile cracks. AE sources for which the shear ratios X are larger than 60% are referred to as shear cracks. For those with shear rations between 40% and 60%, AE sources are classified as mixed-mode. In the eigenvalue analysis, three eigenvectors e_1, e_2, and e_3 are also determined. Theoretically, these are derived as:

$$\begin{aligned} e_1 &= l + n \\ e_2 &= l \times n \\ e_3 &= l - n \end{aligned} \quad (6)$$

Here, vectors l is the crack-motion vector and n is the normal vector to the crack surface, which are interchangeable. In the case of a tensile crack, vector l is parallel to vector n. Thus, vector e_1 could give

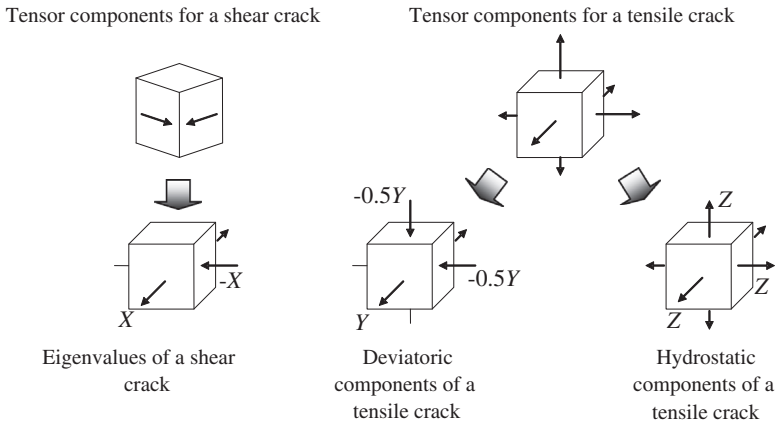

Fig. 6. Unified decomposition of eigenvalues of the moment tensor.

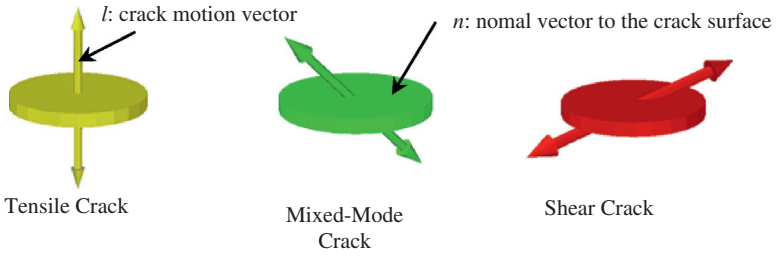

Fig. 7. 3-D models for tensile, mixed-mode and shear cracks.

the direction of the crack-opening, while for a shear crack the sum $e_1 + e_3$ and the difference $e_1 - e_3$ give the two vectors l and n.

In order to visualize AE source kinematics, Light Wave 3D software (New Tek) is applied. Crack models for tensile, mixed-mode and shear cracks are given in Fig. 7. Here, the arrow vector indicates a crack motion vector l, and the circular plate corresponds to a crack surface which is perpendicular to a crack normal vector n.

4. Results and discussion

4.1. AE activity and half-cell potential

Cumulative AE hits and AE events for every 1 h of all 6 channels are shown in Fig. 8. One AE event consists of 6 signals which were detected by all 6 AE sensors and analyzed. AE hits and AE events start to gradually increase during the first 42 days and the calm period of AE activity for a week is observed. The calm period is found after increase of the AE hits and AE events from 35 days to 42 days. In addition, the second increase of AE events was observed at 49 days. Therefore, the culm stage that was observed from 42 days to 49 days corresponds to Phase 2 in Fig. 1. Following the calm phase, AE hits and AE events increase continually. The curve of cumulative AE hits is in good agreement with the curve of corrosion loss in Fig. 1. Thus, it leads to the fact that the onset of corrosion occurred during the first 42 days and the corrosion-induced cracks due to expansion of corrosion products could occur from 49 days to 91 days. Based on these findings, the corrosion process is divided into Stage 1 and Stage 2 as shown in Fig. 8. Here, Stage 1 corresponds to Phase 1 and Phase 2, Stage 2 corresponds to Phase 3 and Phase 4.

Cumulative AE hits are compared with half-cell potentials in Fig. 9. The half-cell potentials start to decrease after 28 days. Then, the potentials keep negative and less than −350 mV in Stage 2. Thus, the increase in AE activity could be associated with the decrease trend of the half-cell potentials. After Stage 1, corresponding to continuous increase in AE activity, corrosion-induced cracks in concrete is to be nucleated due to expansion of corrosion products in rebar. The corrosion could be started from the start. However, the half-cell potentials cannot detect the small corrosion. On the other hand, AE can detect very tiny corrosion phenomenon. That's why AE activities detected from the beginning in Fig. 9.

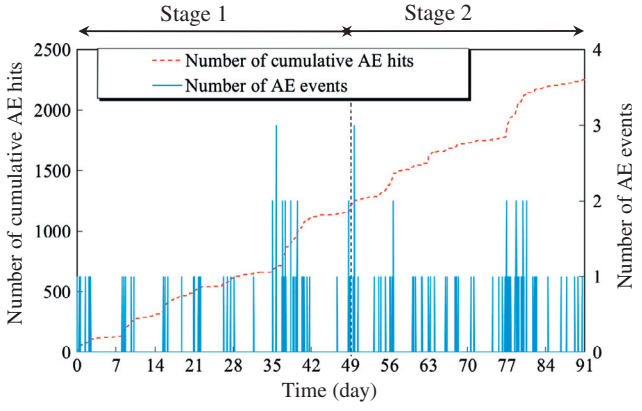

Fig. 8. Number of cumulative AE hits and AE events.

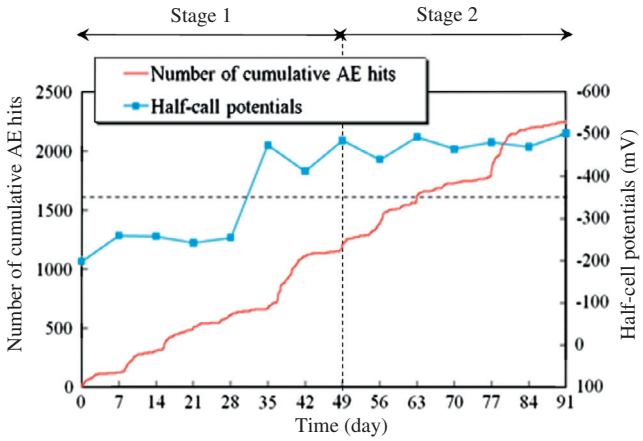

Fig. 9. Number of cumulative AE hits and half-cell potentials.

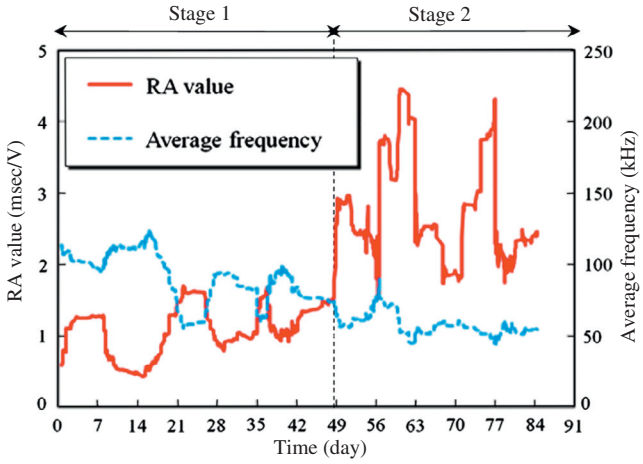

Fig. 10. Variations of RA value and averaged frequency.

4.2. AE parameter analysis

Variations of the RA values and the average frequency are given in Fig. 10. We used 100 points for running average. Although the trend of variation is not clear at Stage 1, the RA values start to increase at Stage 2. From 14 days to 21 days elapsed at Stage 1, an abrupt increase in the RA value and the decrease in the average frequency are observed. This suggests that generation of other than

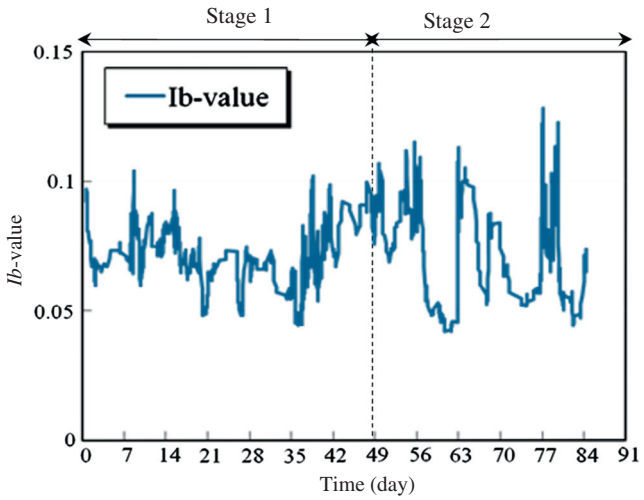

Fig. 11. Variations of *Ib*-value.

tensile cracks [6] due to the onset of corrosion in rebar. Interestingly the decrease of the half-cell potentials in Fig. 9 follows this generation. At Stage 2, the increase in the RA values and the decrease in the average frequency are further observed, suggesting nucleation of corrosion-induced cracks in concrete.

Variation of the *Ib*-values is given in Fig. 11. The large drops observed between 21 days and 35 days, before the first dramatically increase of AE activities in Fig. 8. This might be implied that modest micro-cracks are generated as the onset of corrosion at the surface of the rebar. Due to high AE activity at Stage 2, the *Ib*-values decrease. Since results of *Ib*-values at 56 and 84 days elapsed are comparatively lower than those of the Stage 1, large-scale cracks are considered to be actively generated as corrosion-induced cracks in concrete. Furthermore, fluctuations of *Ib*-values in Stage 2 are even bigger than those of Stage 1. These results imply that cracks were repeatedly generated as the onset of corrosion and the corrosion-induce cracks in concrete.

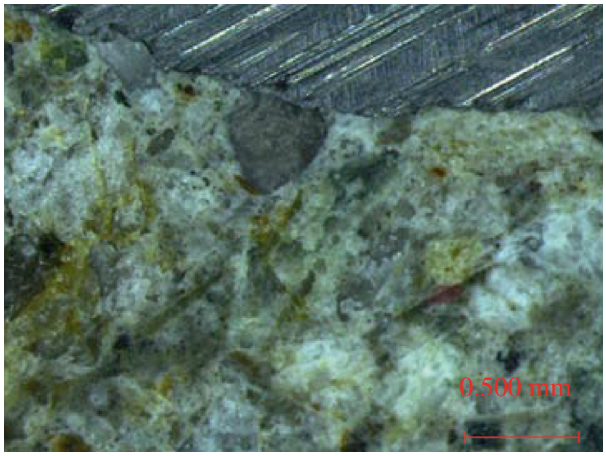

Fig. 14. Results of stereo-microscope at Stage 1.

4.3. SiGMA analysis

In the SiGMA analysis, AE event definition time (EDT) is set to 100 μs, which is applied to recognize AE waves occurring within the specified time from the first-hit and to classify them as part of the current event. Results of SiGMA analysis at Stage 1 and Stage 2 are shown in Figs. 12 and 13. 30 AE events were detected in the Stage 1. These events are located surrounding the rebar and at around the top of the specimen. The events near the rebar could be related with the onset of corrosion. In Stage 2, 19 AE events are determined closely near the rebar. AE events are mostly classified into tensile cracks and mixed-mode cracks, suggesting that cracks extend outward from the rebar. Results of the stereo-microscope observation at Stage 1 and Stage 2 are shown in Figs. 14 and 15. Two specimens for the observation were prepared by terminating the cyclic test at 49 days and 91 days. At Stage 1, corrosion was confirmed at the surface of the rebar in visual observation. However, no cracks were observed in concrete by the stereo-micro-

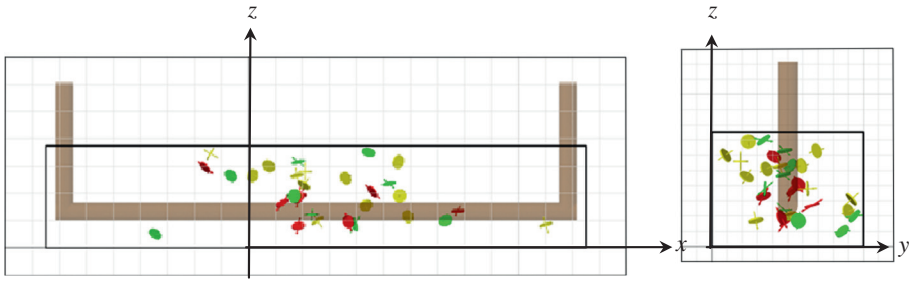

Fig. 12. Results of SiGMA analysis during the first 49 days (Stage 1).

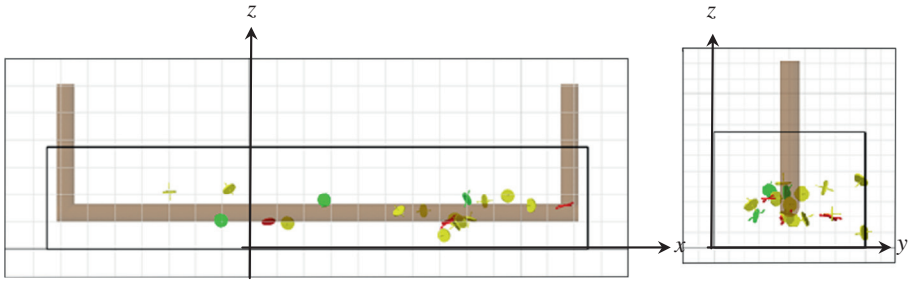

Fig. 13. Results of SiGMA analysis from 49 days to 91 days (Stage 2).

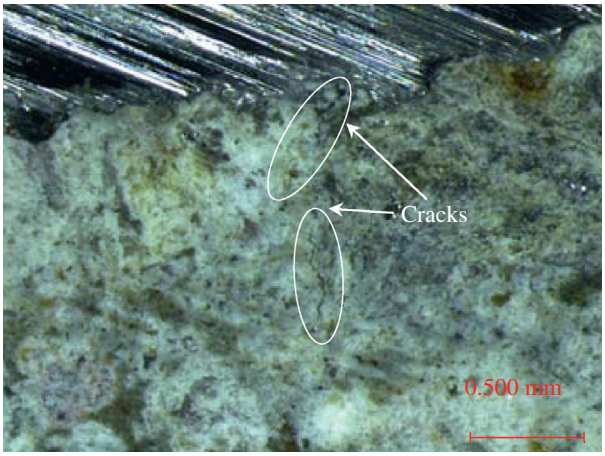

Fig. 15. Results of stereo-microscope at Stage 2.

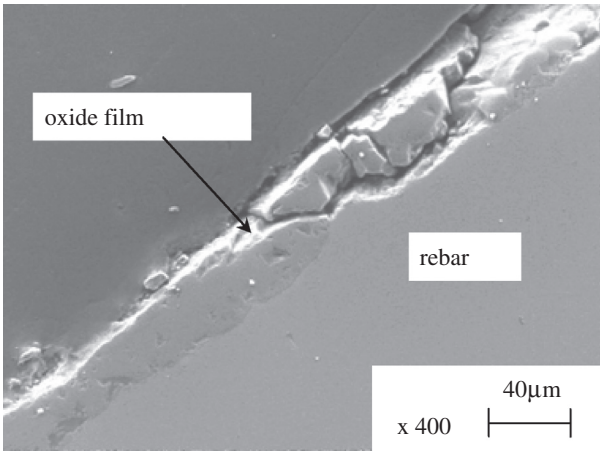

Fig. 16. SEM photo of rebar cross-section at 49 days (Stage 1).

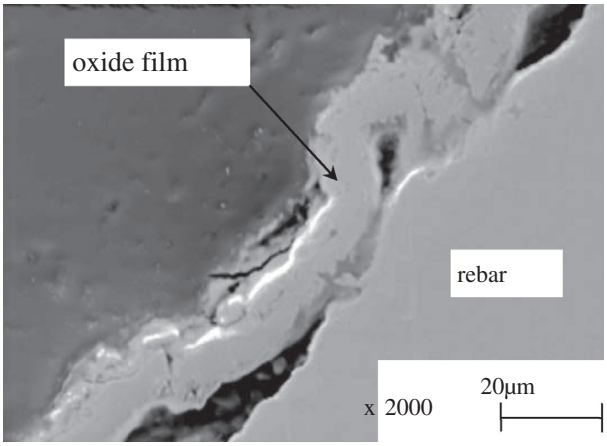

Fig. 18. SEM photo of rebar cross-section at 91 days (Stage 2).

scope as shown in Fig. 14. Thus, it implies that AE phenomena, which were detected during stage 1, occurred due to corrosion initiation in rebar. At Stage 2, the corrosion was observed in whole of rebar. Additionally, micro-cracks are observed at the cross-section as shown in Fig. 15. Thus, agreement between locations of micro-cracks and results of SiGMA analysis is demonstrated. According to the SiGMA analysis in Figs. 13 and 14, both the shear cracks and the mixed-mode cracks are located around rebar at Stage 1, while most cracks are classified into the tensile crack near rebar at Stage 2. It suggests that both shear cracks and mixed-mode cracks due to the corrosion initiation would lead to expansion of corrosion products generation of tensile cracks in concrete.

4.4. SEM and EPMA observations

SEM and EPMA observation of the rebar was con-ducted by removing rebar from the specimens at the two periods after 49 and 91 days elapsed.

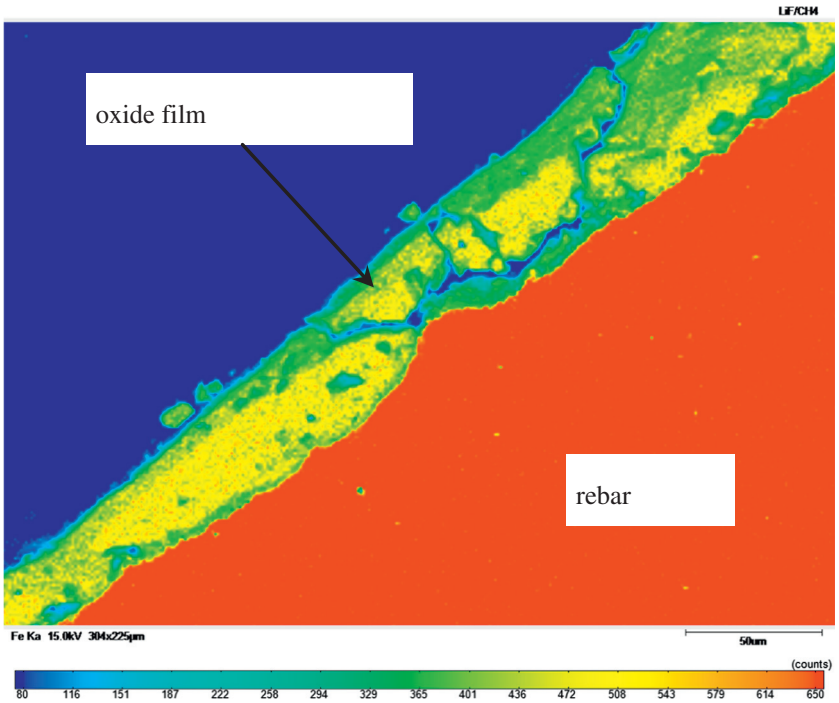

Fig. 17. Mapping image of Fe of rebar on EPMA at 49 days (Stage 1).

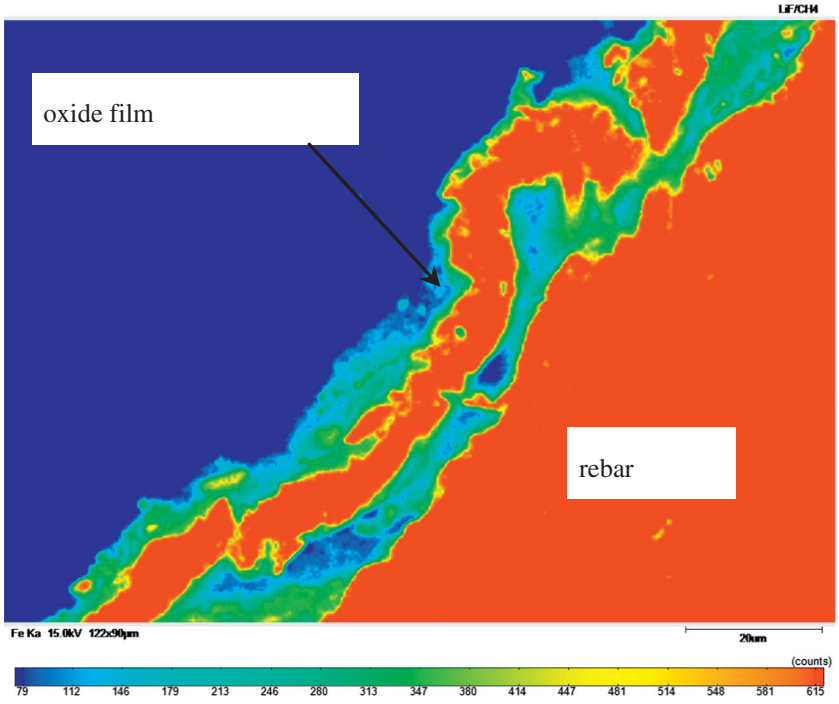

Fig. 19. Mapping image of Fe of rebar on EPMA at 91 days (Stage 2).

EPMA is an analysis method that allows the quantification of elemental concentrations with high spatial resolution and sensitivity on a solid surface as well as the measurement of the area distribution of elements [12].

Both mapping images of concentration of Fe ions of the rebar and SEM after 49 days elapsed are shown in Figs. 16 and 17. During Stage 1, the tiny void is found between the rebar and the oxide film. It implies that the oxide film has been exfoliated due to the onset of corrosion. However, no progress of corrosion inside the rebar is observed in Stage 1. Both mapping images of concentration of Fe ions of the rebar and SEM after 91 days elapsed are shown in Figs. 18 and 19. During Stage 2, the oxide film is completely exfoliated from the surface of rebar, and it is confirmed that the corrosion progresses to inside rebar. Here, Figs. 17 and 19 indicate concentration level of Fe ions. Color gradation mean the concentration levels, which indicate high concentration levels with the increase in brightness.

It implies that during Stage 1, the oxide film on the surface of the rebar is exfoliated. Then, during Stage 2, the oxide film is exfoliated, and rust starts to be generated inside rebar. It is found that only the surface of rebar is corroded due to the onset of corrosion at Stage 1. Thus, the number of both AE hits and AE events are low, and the RA value is low and the average frequency is high. Then the corrosion further penetrates and is nucleated inside the rebar at Stage 2, as corrosion-induced cracks are nucleated in concrete due to expansion of corrosion products. Thus, the number of both AE hits and AE events are high, the RA value becomes high and the average frequency becomes low.

5. Conclusions

Continuous AE monitoring was carried out during the cyclic wet and dry test of reinforced concrete specimens. The following conclusions are obtained.

(1) Two Stages in the corrosion process are con-firmed, in relation to the onset of corrosion in rebar and the nucleation of corrosion-induced cracks in concrete.

(2) At the onset of corrosion, the decrease of the RA value and the increase of the average frequency are observed. At the same time, the decrease of the *Ib*-value is confirmed. It implies that the onset of corrosion could be identified by AE parameter analysis.

(3) Particular AE activity is found at Stage 2, corresponding to Phase 3 and Phase 4 in the phenomenological model. Due to corrosion-induced cracks, many of AE hits are observed. At Stage 2, the in-crease of the RA value and the decrease of the aver-age frequency are observed. Then, the fluctuations of *Ib*-values in the Stage 2 are even bigger than those of Stage 1. This implies that *Ib*-value is effective to detect both the onset of corrosion and the corrosion-induced cracks.

(4) At Stage 1, AE events were located in the specimen while no cracks were observed by the stereo-microscope. It implies that AE phenomena occurred due to corrosion initiation as the shear and the mixed-mode cracks. At Stage 2, micro-cracks were observed at the cross-section by the stereo-microscope. The locations of the AE sources by the SiGMA analysis are agreement with those of the corrosion-induced cracks in concrete, and AE sources are mostly of tensile cracks.

(5) From comparing SEM and EPMA photos with AE activity, it is confirmed that at 49 days AE activity corresponds to the transition from Phase 1 to Phase 2 as the onset of corrosion, and at 91 days elapsed AE activity is associated with the transition from Phase 3 to Phase 4 as the generation of corrosion-induced cracks in concrete.

Acknowledgments

To perform experiments and analyses, the assistance of technical associate, Dr. Yuichi Tomoda was valuable. The research achieved in this paper was financially supported by Kumamoto University Global Centers of Excellence (GCOE) Program: Global

Initiative Center for Pulsed Power Engineering. The authors wish to deeply thank the program.

References

[1] Dubravka B, Dunja M, Dalibor S. Non-destructive corrosion rate monitoring for reinforced. Concrete structures; 2000.
[2] Kawasaki Y, Tomoda Y, Ohtsu M. AE monitoring of corrosion process in cyclic wet–dry test. J Constr Build Mater 2010;24(12):2353–7.
[3] Melchers RE, Li CQ. Phenomenological modeling of reinforcement corrosion in marine environments. ACI Mater J 2006;103(1):25–32.
[4] Aggelis Dimitrios G. Classification of cracking mode in concrete by acoustic emission parameter. J Mech Res Commun 2011;38:153–7.
[5] Shiotani T, Ohtsu M, Ikeda K. Detection and evaluation of AE waves due to rock deformation. J Constr Build Mater 2001;15(5–6):235–46.
[6] Yokota M. Study on corrosion monitoring of reinforcing steel bars in 36 years-old actual concrete structures. Concr Lib JSCE 1999;33:155–64.
[7] ASTM C876. Standards test method for half-cell potentials of uncoated reinforcing steel in concrete. Annual book of ASTM standard; 1991.
[8] Ohtsu M. Test method for clarification of active cracks in concrete structures by AE. Mater Struct 2010;43:1187–9.
[9] Ohtsu M, Okamoto T, Yuyama S. Moment tensor analysis of acoustic emission for cracking mechanisms in concrete. ACI Struct J 1991;95(2):87–95.
[10] Kawasaki Y, Kobarai T, Ohtsu M. Kinematics of corrosion damage monitored by acoustic emission techniques and based on a phenomenological model. J Adv Concr Technol 2012;10:160–9.
[11] Ohtsu M. Simplified moment tensor analysis and unified decomposition of acoustic emission source. J Geophys Res 1991;96(B4):6211–21.
[12] Mori D, Yamada K. A review of recent applications of EPMA to evaluate the durability of concrete. J Adv Concr Technol 2007;5(3):285–98.